Available online at www.sciencedirect.com

ScienceDirect

Journal of Hazardous Materials 153 (2008) 285–292

Journal of Hazardous Materials

www.elsevier.com/locate/jhazmat

Crystal chemistry of sodium zirconium phosphate based simulated ceramic waste forms of effluent cations (Ba^{2+}, Sn^{4+}, Fe^{3+}, Cr^{3+}, Ni^{2+} and Si^{4+}) from light water reactor fuel reprocessing plants

O.P. Shrivastava *, Rashmi Chourasia

Department of Chemistry, Dr. H.S. Gour University, Sagar 470003, India

Received 21 May 2007; received in revised form 20 August 2007; accepted 20 August 2007
Available online 25 August 2007

Abstract

A novel concept of immobilization of light water reactor (LWR) fuel reprocessing waste effluent through interaction with sodium zirconium phosphate (NZP) has been established. Such conversion utilizes waste materials like zirconium and nickel alloys, stainless steel, spent solvent tri-butyl phosphate and concentrated solution of $NaNO_3$. The resultant multi component NZP material is a physically and chemically stable single phase crystalline product having good mechanical strength. The NZP matrix can also incorporate all types of fission product cations in a stable crystalline lattice structure; therefore, the resultant solid solutions deserve quantification of crystallographic data. In this communication, crystal chemistry of the two types of simulated waste forms (type I—$Na_{1.49}Zr_{1.56}Sn_{0.02}Fe_{0.28}Cr_{0.07}Ni_{0.07}P_3O_{12}$ and type II—$Na_{1.35}Ba_{0.14}Zr_{1.56}Sn_{0.02}Fe_{0.28}Cr_{0.07}Ni_{0.07}P_{2.86}Si_{0.14}O_{12}$) has been investigated using General Structure Analysis System (GSAS) programming of the X-ray powder diffraction data. About 4001 data points of each have been subjected to Rietveld analysis to arrive at a satisfactory structural convergence of Rietveld parameters; R-pattern (R_p) = 0.0821, R-weighted pattern (R_{wp}) = 0.1266 for type I and R_p = 0.0686, R_{wp} = 0.0910 for type II. The structure of type I and type II waste forms consist of ZrO_6 octahedra and PO_4 tetrahedra linked by the corners to form a three-dimensional network. Each phosphate group is on a two-fold rotation axis and is linked to four ZrO_6 octahedra while zirconium octahedra lies on a three-fold rotation axis and is connected to six PO_4 tetrahedra. Though the expansion along c-axis and shrinkage along a-axis with slight distortion of bond angles in the synthesized crystal indicate the flexibility of the structure, the waste forms are basically of NZP structure. Morphological examination by SEM reveals that the size of almost rectangular parallelepiped crystallites varies between 0.5 and 1.5 μm. The EDX analysis provides the analytical evidence of immobilization of effluent cations in the matrix. The particle size distributions of the material along selected reflecting planes have been calculated by Scherrer's formula.

Keywords: NZP ceramics; X-ray powder diffraction; Rietveld refinement; GSAS; Radwaste immobilization

1. Introduction

Sodium zirconium phosphate related compounds can be synthesized by various conventional and novel ceramic methods such as high temperature solid state reaction, single crystal formation, hydrothermal synthesis, co-precipitation, microwave sintering, etc. [1–6]. The NZP structure is basically a three-dimensional network of $(Zr_2P_3O_{12})^-$ units resulting in a flexible hexagonal crystal structure formed by corner sharing of PO_4 tetrahedra with ZrO_6 octahedra along c-axis. In the three-dimensionally linked interstitial spaces the alkali atoms such as Na, K, Ca, Ba, Mg, Sr, etc. can be located in the holes between ZrO_6 octahedra. The octahedral site in NZP is occupied by Zr^{4+} and tetrahedral site is occupied by P^{5+} and the two interstitial sites may be occupied by Na^+. The site I has distorted octahedral coordination whereas site II has trigonal prismatic coordination. Several divalent cations substitute for two alkali ions and rare earth elements are assumed to occupy the Zr^{4+} site. The strongly bonded but open structure allows the high mobility of alkali ions tunneling through the PO_4–ZrO_6 polyhedra chain. As a result there are enormous numbers of compounds containing 1–5 different cations, belonging to this family [7–10]. Hawkins and Scheetz [11], Seida et al. [12] and Troole et al. [13] have reported that the immobilization of trivalent elements into Zr position was

* Corresponding author. Tel.: +91 7582264249.
E-mail address: dr_ops11@rediffmail.com (O.P. Shrivastava).

0304-3894/$ – see front matter © 2007 Elsevier B.V. All rights reserved.
doi:10.1016/j.jhazmat.2007.08.057

questionable but in the light of various publications [8,14–25] on immobilization of trivalent cations in NZP matrix the final word on the mechanism of solids state reactivity of trivalent elements requires more experimental evidence and better theoretical model. The NZP compounds are receiving attention for their potential applications in anti thermal shock devices, space technology, automobile industry, etc. They are also well known for their applications as catalyst supporters, fast ion conductors and host for immobilizing radioactive waste. Recently members of NZP structural family have been proposed as host materials for rare earths and actinides [26,27].

The primary objective of this research has been to demonstrate the feasibility of conversion of light water reactor fuel reprocessing radioactive waste into a single phase crystalline ceramic material of stable lattice structure which possesses a high leach resistance appropriate for geological disposal eliminating the need of additional barriers. Immobilization of high level nuclear waste in NZP matrix was firstly proposed by Roy et al. on account of numerous advantages: high stability of three-dimensional network, high waste loading, refractory nature, easy method of synthesis and stability towards radiation damage and dissolution [28–30]. Two major types of formulations of simulated NZP waste forms have been synthesized in the laboratory by Hirose et al. [31]. Their chemical compositions are as follows:

Type I $Na_{1.49}Zr_{1.56}Sn_{0.02}Fe_{.28}Cr_{0.07}Ni_{0.07}P_3O_{12}$ Mol. wt. 487.20
Type II$Na_{1.35}Ba_{0.14}Zr_{1.56}Sn_{0.02}Fe_{0.28}Cr_{0.07}Ni_{0.07}P_{2.86}Si_{0.14}O_{12}$Mol. wt. 502.80

It is in this background that the complete crystallographic characterization of such simulated waste-forms becomes interesting for process engineering and system development for immobilization of light water reactor's low level waste effluents in NZP matrix.

2. Experimental

2.1. Oxide route synthesis of type I and type II NZP ceramic phases

Stoichiometric amounts of dry fine powders of precursor oxides/carbonates and ammonium dihydrogen phosphate were mixed in a mortar-pestle in glycerol medium. The selected chemical compounds were AR grade Na_2CO_3, ZrO_2, Fe_2O_3, SnO_2, $Ni(NO_3)_26H_2O$, Cr_2O_3 for type I and additionally $BaCO_3$ and SiO_2 for type II sample, respectively. The glycerol paste was gradually heated initially at 600 °C for 8 h in a platinum crucible. The initial heating is done to decompose Na_2CO_3 and $(NH_4)H_2PO_4$ with the emission of carbon dioxide gases, ammonia and water vapors. The mixture was reground to micron size, pressed into pellets at room temperature and sintered in a platinum crucible at 1000 °C for 72 h.

2.2. Characterization

The X-ray diffraction pattern has been recorded between $2\theta = 10–90°$ on a Rigaku RUH3R diffractometer using Cu Kα radiation at step size of $2\theta = 0.02°$ and a fixed counting time of 2 s/step. The X-ray data was subjected to General Structure Analysis System (hereafter GSAS) software programming

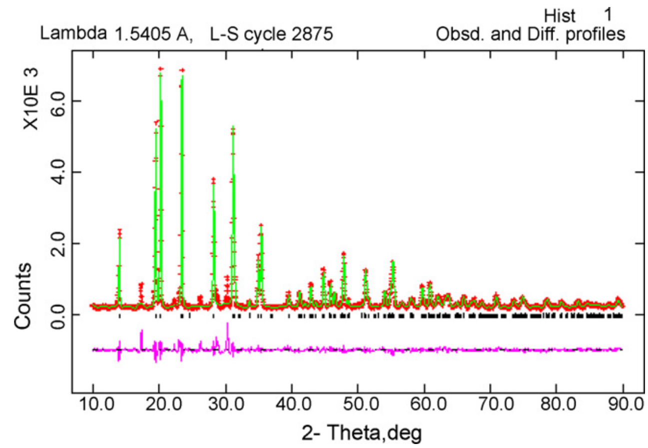

Fig. 1. Rietveld refinement pattern of type I ceramic powder. The '+' are the raw X-ray diffraction data, and the overlapping continuous line is the calculated pattern. Black vertical lines in the profile indicate the position of the allowed reflections for Cu Kα1 and Cu Kα2. The curve at the bottom is the difference in the observed and calculated intensities in the same scale.

which is capable of handling and refining the step analysis powder diffraction data in a comprehensive manner. Scanning electron microscopy (SEM) has been carried out on a HITACHI S-3400n electron microscope system attached with Thermonoran ultra dry detector facility for energy dispersive X-ray (EDX) analysis.

3. Result and discussion

The diffraction patterns of type I and type II ceramic waste forms are typical characteristic of the NZP based structure. They can be indexed assuming a rhombohedral cell ($R-3c$) as also reported elsewhere [32]. The rule for the rhombohedral lattice: $-h+k+l=3n$ has been verified for all reflections between $2\theta = 10–90°$. The intensity and positions of the diffraction pattern fairly matched with the reported standard pattern of sodium zirconium phosphate which gives six intense absorptions between $2\theta = 19.46–35.30°$ (Figs. 1 and 2) [33]. The Rietveld refinement of the step scan data was performed by the least square method [34]. The refinement converges to a satisfac-

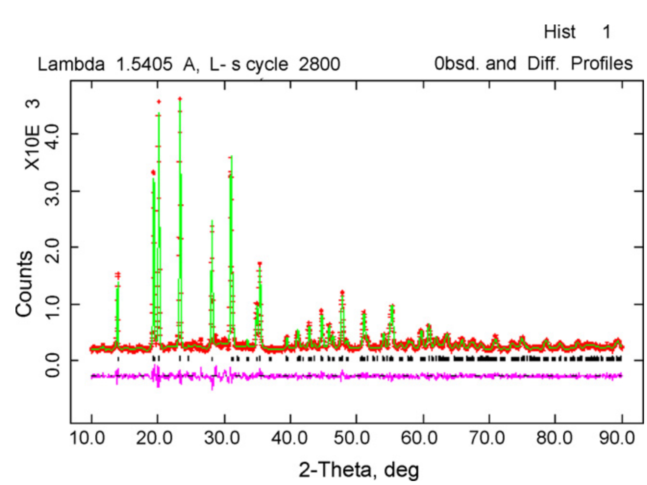

Fig. 2. Rietveld refinement pattern of type II ceramic powder.

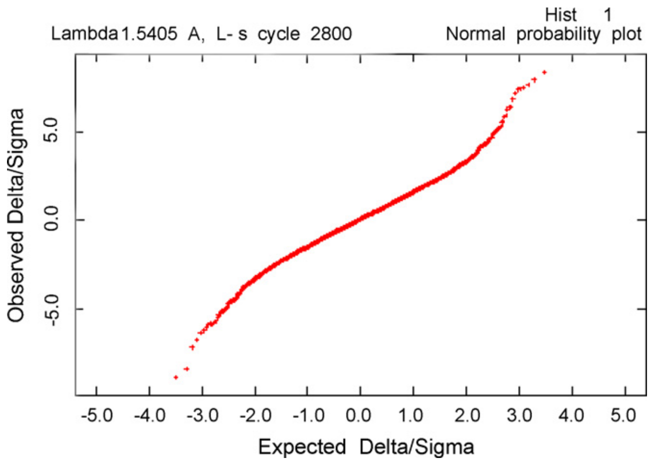

Fig. 3. Probability plot between I_o–I_c for polycrystalline type II ceramic sample.

tory structure fit giving $R_p = 0.0821$ and 0.0686 for type I and II phases, respectively. The normal probably plot for the histogram gives nearly a straight line indicating that the observed intensity (I_o) and calculated intensity (I_c) values are for the most part normally distributed (Fig. 3). The lattice parameter are close to the corresponding values for NZP [35]. The cell parameters of the two specimens register slight increase in c direction (Table 1). The presence of the bulkier cations on M_1 site instead of comparatively small Na^+ in the interstices increases the size of NaO_6 distorted octahedra and hence stretches the bridging PO_4 tetrahedra in the c direction. Simultaneously the structure shows a contraction along a direction. This is due to bond angle distortions as a result of the coupled rotation of ZrO_6 and PO_4

Table 1
Crystallographic data for type I and type II ceramic phases

Phase	Type I	Type II
Lattice parameters		
$a = b$	8.79326 (20)	8.78103 (19)
c	22.8826 (9)	22.8084 (9)
$\alpha = \beta = 90°$		
$\gamma = 120°$		
R-pattern (R_p)	0.0821	0.0686
R-weighted pattern (R_{wp})	0.1266	0.0910
R_{wp} expected (R_e)	0.0506	0.0546
R-structure factor (RF^2)	0.06806	0.05284
Volume of unit cell (Å^3)	1525.57 (6)	1523.06 (5)
Density$_{calculated}$ (gm/cm^3)	3.269	3.107
Density$_{expected}$ (gm/cm^3)	3.120	2.912
Unit cell formula weight	3003.517	2849.445
S (goodness-of-fit)	2.51	1.67
Slope	1.8781	1.5673
No. of parameters refined	33	36

Structure: rhombohedral; space group: $R{-}3c$; $Z = 6$.

$$R_p = \frac{\sum y_i(\text{obs}) - y_i(\text{cal})}{\sum y_i(\text{obs})} \qquad R_{wp} = \left\{ \frac{\sum w_i(y_i(\text{obs}) - y_i(\text{cal}))^2}{\sum w_i(y_i(\text{obs}))^2} \right\}$$

$$R_e = \left[\frac{N - P}{\sum w_i y_{oi}^2} \right]^{1/2} \qquad S = \frac{R_{wp}}{R_{exp}}$$

$y_{i(o)}$ and $y_{i(c)}$ are observed and calculated intensities at profile point i, respectively. w_i is a weight for each step i. $I_{k(o)}$ and $I_{k(c)}$ are observed and calculated integrated intensities, respectively. N is the no. of parameters refined.

Table 2
Refined atomic coordinates of type I and type II polycrystalline ceramic powders at room temperature

Atom	x	y	z	Occupancy	Uiso (Å^2) (isotropic thermal parameter)
$Na_{1.492}Zr_{1.56}Sn_{0.02}Fe_{28}Cr_{0.07}Ni_{0.07}P_3O_{12}$					
Na1	0.0	0.0	0.0	1.0	0.07779
Na2	0.0	0.0	0.502	0.01068	0.07773
Zr3	0.0	0.0	0.14541	0.85514	0.03002
Sn31	0.0	0.0	0.14541	0.02251	0.03742
Fe32	0.0	0.0	0.14541	0.13522	0.04055
Cr33	0.0	0.0	0.14541	0.03715	0.04187
Ni34	0.0	0.0	0.14541	0.03076	0.05027
P5	0.29184	0.0	0.25	0.98094	0.03274
O6	0.18083	−0.0232	0.19528	1.05295	0.04403
O7	0.19073	0.17205	0.0875	1.05157	0.04403
$Na_{1.35}Ba_{0.14}Zr_{1.56}Sn_{0.02}Fe_{28}Cr_{0.07}Ni_{0.07}P_{2.86}Si_{0.14}O_{12}$					
Na1	0.0	0.0	0.0	1.0	0.05666
Ba12	0.0	0.0	0.0	0.00336	0.06565
Na2	0.0	0.0	0.501	0.0453	0.05666
Zr3	0.0	0.0	0.14589	0.79538	0.00938
Sn31	0.0	0.0	0.14589	0.00844	0.02985
Fe32	0.0	0.0	0.14589	0.13903	0.03722
Cr33	0.0	0.0	0.14589	0.04186	0.02857
Ni34	0.0	0.0	0.14589	0.02864	0.025
P4	0.2891	0.0	0.25	0.92607	0.01238
Si51	0.2891	0.0	0.25	0.05265	0.03219
O5	0.17751	−0.03006	0.1956	0.98171	0.02408
O6	0.1933	0.16611	0.0874	0.98222	0.02408

Isotropic atomic displacement factor = $\exp(-8\pi^2 B \sin^2\theta/\lambda^2)$.

Table 3
Inter-atomic distances (Å) for type I and type II ceramic powder

Type I		Type II	
Na1_O6	2.55700(14)*6	Na1_O6	2.55082(7)*6
Na2_O6	2.52164(7)*3	Na2_O6	2.53304(7)*3
Na2_O6	2.59268(7)*3	Na2_O6	2.56869(7)*3
Zr3_O5	2.04573(4)*3	Zr3_O5	2.04847(4)*3
Zr3_O6	2.07485(4)*3	Zr3_O6	2.07667(4)*3
P4_O5	1.53287(4)*2	P4_O5	1.52010(3)*2
P4_O6	1.531350(30)*2	P4_O6	1.55143(3)*2
Na1_Na2	0.04556(0)*2	Na1_Na2	3.99677(7)*6
Na2_Na2	0.09113(0)	Na1_Na2	0.02281(0)*2
Na1_Zr3	3.31283(14)*2	Na1_Zr3	3.32752(14)*2
Na2_Zr3	3.26727(14)*2	Na2_Na2	0.04562(0)
		Na2_Zr3	3.30471(13)
		Na2_Zr3	3.35033(14)

The * denotes multiplicity of bonds and angles. The values in parentheses denotes (esd) estimated standard deviation values.

polyhedra [36]. Alteration in lattice parameters shows that the network slightly modifies its dimensions to accommodate the cations occupying M_1 and M_2 sites without breaking the bonds. The basic framework of NZP accepts the cations of different sizes and oxidation states to form solid solutions but at the same time retaining the overall geometry unchanged. The final atomic coordinates and isotropic thermal parameters (Table 2), inter-atomic distances (Table 3), bond angles (Table 4) and structure factors of prominent reflections (Table 5) are extracted from the crystal information framework prepared after final cycle of refinement.

Fig. 4 illustrates that the structure is based on a 3D framework built from ZrO_6 octahedra and corner sharing PO_4 tetrahedra. The Zr–O distances of the octahedra and P–O distances of the tetrahedra are comparable with those found by Shannon and Prewitt [37]. Other calculated M–O distances also fit in the proposed model. The Oak Ridge Thermal Ellipsoid Plot Program (ORTEP) view generated by the refined structural data shows two values of Zr–O distances namely Zr(3)–O(5) and Zr(3)–O(6) in multiple of 3 whereas P–O distances occur in two pairs. The bond angle data reveals that the planar O–Zr–O angles are different from those connecting the apex oxygen atoms of the octahedron (Fig. 5). The O(5)–Zr(3)–O(6) bond angle is 173.91 (average of 174.20 in type I and 173.63 in type II) indicating that the ZrO_6 octahedra are slightly tilted. Likewise the

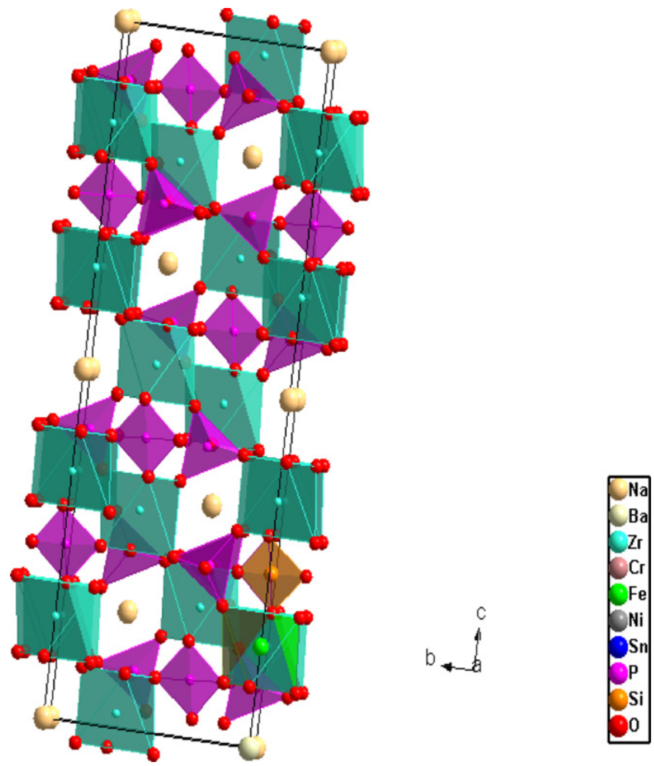

Fig. 4. DIAMOND view of stick and ball representation of coordination sites of Na/Ba, Zr/Fe/Cr/Ni/Sn and P/Si for type II.

Table 4
O–M–O bond angles in type I and type II ceramic materials

Type I		Type II	
O6_Na1_O6	65.6884(21)*6	O6_Na1_O6	65.411(21)*6
O6_Na1_O6	180*2	O6_Na1_O6	179.9802
O6_Na1_O6	114.3116(2)*6	O6_Na1_O6	114.589(21)*6
O6_Na2_O6	66.7288(21)*3	O6_Na1_O6	179.972(0)
O6_Na2_O6	178.7214*2	O6_Na1_O6	179.9657
O6_Na2_O6	114.2934(2)*6	O6_Na2_O6	65.928(21)*3
O6_Na2_O6	64.6733(21)*3	O6_Na2_O6	179.3608(0)*2
O5_Zr3_O5	92.1431(17)*3	O6_Na2_O6	179.3614
O5_Zr3_O6	92.3297(18)*3	O6_Na2_O6	114.5843(21)*6
O5_Zr3_O6	174.20689(10)*3	O6_Na2_O6	64.9001(21)*3
O5_Zr3_O6	91.3665(19)*2	O5_Zr3_O5	92.3196(17)
O5_Zr3_O6	91.3666(19)	O5_Zr3_O6	92.2179(18)*3
O6_Zr3_O6	83.8854(20)	O5_Zr3_O6	91.9579(18)*3
O5_P4_O5	110.4615(25)	O5_Zr3_O6	173.63251(10)*2
O5_P4_O6	107.26330(30)*2	O5_Zr3_O6	173.63240(10)
O5_P4_O6	112.3834(10)	O6_Zr3_O6	83.1639(19)*3
O5_P4_O6	112.3835(10)	O5_P5_O5	112.1940(24)
O6_P4_O6	107.1069	O5_P5_O6	104.08210(20)*2
		O5_P5_O6	113.0937(10)*2
		O6_P5_O6	110.5409

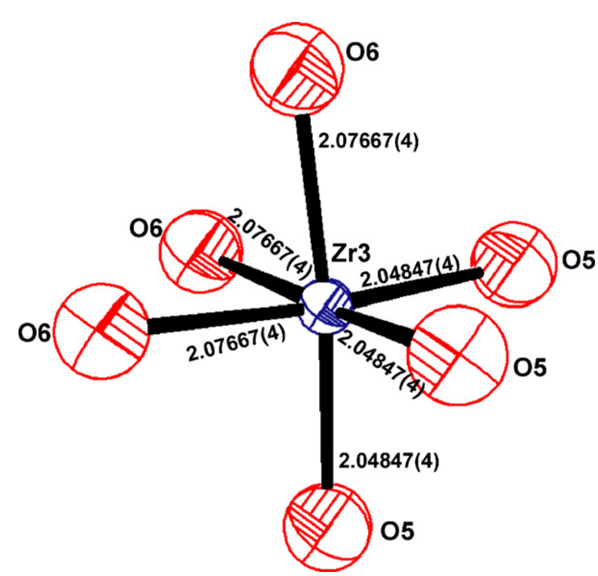

Fig. 5. ORTEP view of Zr coordination in ZrO_6 with their respective bond lengths.

Table 5
Observed and calculated structure factors of polycrystalline type I and type II ceramic phases

h	*k*	*l*	*d*-Space	Fosq	Fcsq	Intensity % (*I* 100)
Type I						
1	0	−2	6.33082	1.973E+05	1.940E+05	26.8339
1	0	−2	6.33082	2.027E+05	1.940E+05	13.7158
1	0	4	4.56103	1.137E+06	1.121E+06	81.7751
1	0	4	4.56103	1.125E+06	1.121E+06	40.2826
1	1	0	4.39663	1.469E+06	1.459E+06	98.4462
1	1	0	4.39663	1.468E+06	1.459E+06	48.9551
1	1	3	3.80496	9.822E+05	9.449E+05	100.0000
1	1	3	3.80496	9.579E+05	9.449E+05	48.5377
2	0	−4	3.16541	1.601E+06	1.510E+06	57.7874
2	0	−4	3.16541	1.643E+06	1.510E+06	29.5079
1	1	6	2.87373	1.588E+06	1.429E+06	96.0410
1	1	6	2.87373	1.568E+06	1.429E+06	47.1897
2	1	1	2.85557	2.022E+05	1.962E+05	12.0860
2	1	4	2.56889	4.866E+05	4.676E+05	24.0577
2	1	4	2.56889	4.865E+05	4.676E+05	11.9752
3	0	0	2.53839	1.737E+06	1.723E+06	42.0532
3	0	0	2.53839	1.719E+06	1.723E+06	20.7152
2	0	8	2.28052	5.254E+05	3.828E+05	10.5476
2	1	−8	2.02439	6.975E+05	6.753E+05	22.8908
2	1	−8	2.02439	6.860E+05	6.753E+05	11.2099
3	1	−4	1.98030	4.812E+05	4.388E+05	15.2281
2	0	−10	1.95501	6.665E+05	6.387E+05	10.3252
0	0	12	1.89855	4.636E+05	4.953E+05	32.5216
2	2	6	1.90248	1.078E+06	1.086E+06	15.9051
2	1	10	1.78637	1.042E+06	1.009E+06	27.9140
2	1	10	1.78637	1.033E+06	1.009E+06	13.7872
3	1	8	1.69644	5.484E+05	4.767E+05	13.5518
3	2	4	1.67024	5.618E+05	5.803E+05	13.5528
4	1	0	1.66177	1.136E+06	1.201E+06	27.1981
4	1	0	1.66177	1.135E+06	1.201E+06	13.5343
3	1	−10	1.54888	7.858E+05	7.596E+05	16.9231
2	0	14	1.49639	1.028E+06	9.772E+05	10.5303
2	1	−14	1.41659	5.488E+05	5.330E+05	10.3981
5	1	4	1.32992	6.486E+05	5.812E+05	11.2785
Type II						
1	0	−2	6.32695	1.314E+05	1.284E+05	26.2476
1	0	−2	6.32695	1.350E+05	1.284E+05	13.4227
1	0	4	4.56207	6.827E+05	6.679E+05	70.6914
1	0	4	4.56207	6.951E+05	6.679E+05	35.8094
1	1	0	4.39051	1.042E+06	1.045E+06	99.8429
1	1	0	4.39051	1.038E+06	1.045E+06	49.4961
1	1	3	3.80207	6.972E+05	6.966E+05	99.9999
1	1	3	3.80207	6.890E+05	6.966E+05	49.1686
2	0	−4	3.16347	1.117E+06	1.187E+06	55.2563
2	0	−4	3.16347	1.155E+06	1.187E+06	28.4347
1	1	6	2.87388	1.133E+06	1.127E+06	92.3432
1	1	6	2.87388	1.136E+06	1.127E+06	46.0574
2	1	1	2.85171	1.771E+05	1.708E+05	14.2058
2	1	4	2.56663	3.151E+05	2.896E+05	20.4267
3	0	0	2.53486	1.452E+06	1.346E+06	45.8728
3	0	0	2.53486	1.458E+06	1.346E+06	22.9165
2	1	−8	2.02416	5.524E+05	5.411E+05	22.1757
2	1	−8	2.02416	5.709E+05	5.411E+05	11.4014
3	1	−4	1.97815	3.535E+05	3.593E+05	13.5489
2	2	6	1.90104	1.005E+06	9.613E+05	35.5867
2	2	6	1.90104	9.957E+05	9.613E+05	17.5396
2	1	10	1.78666	8.517E+05	8.319E+05	26.6564
2	1	10	1.78666	8.663E+05	8.319E+05	13.4901
3	1	8	1.69559	4.007E+05	4.064E+05	11.3154
4	1	0	1.65946	1.059E+06	1.064E+06	28.6771
4	1	0	1.65946	1.090E+06	1.064E+06	14.6803
3	1	−10	1.54853	6.960E+05	6.825E+05	16.4971
2	0	14	1.49750	9.342E+05	9.882E+05	10.3947
2	1	−14	1.41733	5.360E+05	4.866E+05	10.7801
5	1	4	1.32825	6.654E+05	6.234E+05	11.9425

The seven columns within each group contain the values *h*, *k*, and *l*, *d*-spacing, structure factor Fosq (observed), Fcsq (calculated) and intensity, respectively. The reflection selected from the crystallographic information framework (CIF) output of the final cycle of the refinement. Intensities less than 10% were omitted.

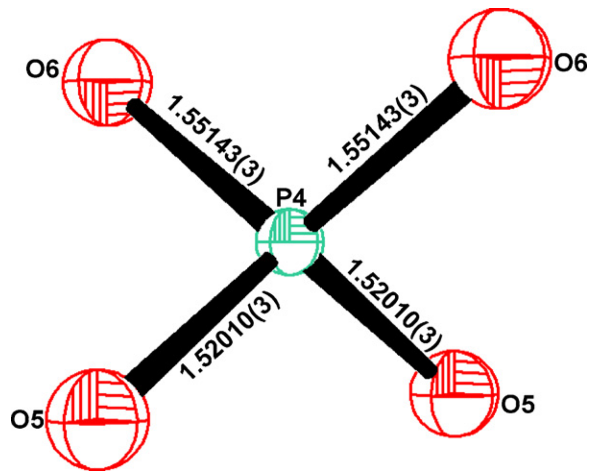

Fig. 6. ORTEP view of P coordination in PO_4 with their respective bond lengths.

PO_4 tetrahedra are also slightly distorted (Fig. 6), with a small deviation of angles from 106° to values between 104° and 113°, but the mean P–O distance 1.535 Å is close to the value found in parent compound $NaZr_2(PO_4)_3$ (1.543 Å) [38].

X-ray data for type I and type II samples was used for the estimation of particle size using Scherrer's formula [39]: $t = 0.9\lambda/\beta\cos\theta$, where t is the crystallite size as measured perpendicular to the reflecting plane, $K = 0.9$, the Scherrer constant, λ the wavelength of X-ray radiation, β the full width at the half intensity of maxima, measured in radians and θ the Bragg angle. The ($h\,k\,l$) values corresponding to prominent reflections, their half width, and particle size for crystals are shown in Table 6. The particle size distribution along the reflecting planes mentioned in table, ranges between 36 and 166 nm for type I and 29 and 235 nm for type II formulations, respectively. The microstructure of the waste forms has been examined by scanning electron microscopy and EDX analysis of the two specimens at two different locations. The evolution of solid mono phase can be seen clearly in the electron micrograph of type I and type II waste forms (Fig. 7a and b) which have rectangular parallelepiped crystallites of 0.5–1.5 μm diameter. Within the limits of experimental error the EDX analytical data on atomic and wt.% of Na, Zr, P and the respective effluent cations in the waste forms match with their corresponding expected molar ratios (Fig. 8).

Table 6
Distribution of particle size along prominent reflecting planes of type I and type II ceramic powder

$h\,k\,l$	Type I		Type II	
	Peak width (2θ)	Particle size (nm)	Peak width (2θ)	Particle size (nm)
1 0 −2	0.16	66.4856	0.182	56.504
1 0 4	0.18	41.895	0.20	235.04
1 1 0	0.18	57.514	0.18	55.7005
1 1 3	0.16	75.8327	0.18	70.730
1 1 6	0.22	36.4355	0.26	29.760
2 1 4	0.24	166.84	0.34	126.6108
3 0 0	0.24	82.87	0.28	74.4631
0 0 12	0.34	63.355	0.36	66.60
3 1 −4	0.32	42.062	0.44	35.5204

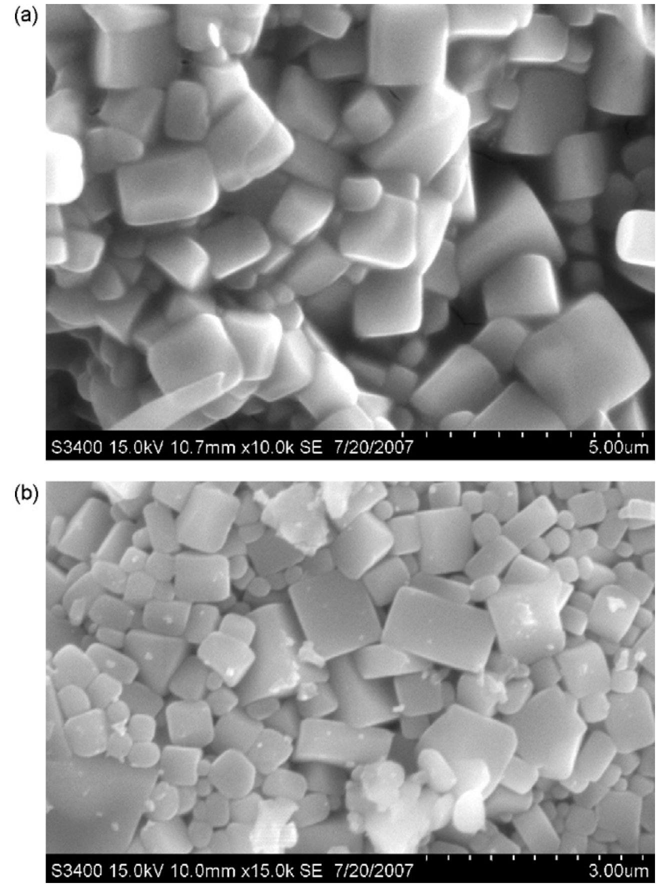

Fig. 7. (a) Scanning electron microphotograph of type I waste form. (b) Scanning electron microphotograph of type II waste form.

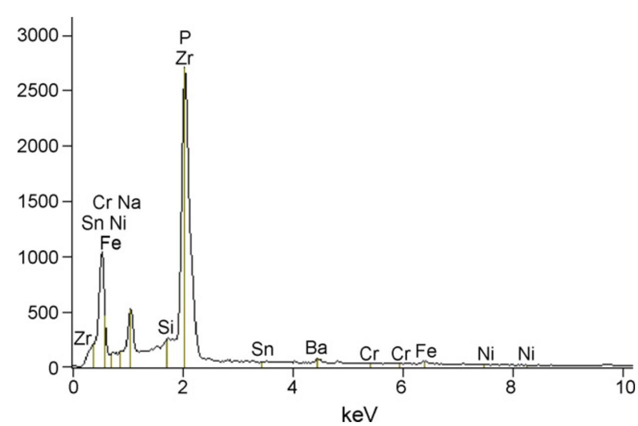

Fig. 8. EDX spectrum of polycrystalline type II ceramic waste form.

The EDX spectrum shows that the effluent cations are crystallochemically present in the NZP matrix.

4. Conclusions

Refinements of powder X-ray diffraction data shows that the solid solutions of type I and type II NZP ceramic phases crystallize in the rhombohedral ($R{-}3c$ space group) structure. Crystal data and structural parameters of the multi component materials have been refined to satisfactory convergence with reasonable values of Rietveld parameters. The calculated values of P–O and Zr–O bond lengths in the waste forms are in agreement with their expected values 1.57 and 2.12, respectively. The O–M–O bond angle data shows that ZrO_6 octahedra and PO_4 tetrahedra in both type I and type II ceramic phases are slightly tilted. The NZP ceramic precursor appears to be a potential material for immobilization and solidification of multivalent ions from low level waste from LWR fuel reprocessing. The proposed structure model also calculated the atomic distances of this cost effective immobilization matrix for low level nuclear waste of the fuel reprocessing plants. The waste forms could be successfully formulated utilizing waste material such as zirconium alloy, stainless steel, nickel alloy, spent solvent, tributyl phosphate (TBP) and concentrated solution of $NaNO_3$ in a minimum amount of additional chemicals.

Acknowledgements

The authors thankfully acknowledge the financial assistance for the research project no. SR/S3/ME/20/2005-SERC-Engg. under its SERC scheme. We also thank the director and staff of U.G.C.-D.A.E consortium for scientific research Indore, India, and the head, Department of Metallurgical Engineering and Material Science, I.I.T. Mumbai, India, for providing X-ray and SEM/EDX facilities, respectively.

References

[1] G.R. Miller, B.J. Mcentire, T.D. Hadnagy, J.R. Rassmussen, S. Gordon, A.V. Virkar, Processing and properties of sodium-beta alumina and NASICON ceramic electrolytes, in: P.A. Vashishta, J.N. Mundy, G.K. Shenoy (Eds.), Proc. Intl. Conf. Fast Ion Transport in Solids: Electrodes and electrolytes, Elsevier North Holland, Inc., New York, NY, 1979, pp. 83–86.

[2] A. Clearfield, P. Jirustithipong, R.N. Cotman, S.P. Pack, Synthesis of sodium di-zirconium triphosphate from alpha-zirconium phosphate, Mater. Res. Bull. 15 (1980) 1603–1610.

[3] S. Barth, M. Andratschke, A. Feltz, C. Jager, Structure and properties of the NASION compounds $Na_3MgZr(PO_4)_3$, $Na_3MnZr(PO_4)_3$ and $Na_{1+x}Zr_2(SiO_{4x}(PO_4)_{3-x})$, Sci. Ceram. 14 (1989) 401–406.

[4] M.B. Sljukic, M.B. Matkovic, B. Prodic, S. Scavnicar, Preparation and crystallographic data of phosphates with common formula $M^IM_2^{IV}(PO_4)_3$ (M^I = Li, Na, K, Rb, Cs; M^{IV} = Zr, Hf), Croatica Chem. Acta 39 (1967) 145–148.

[5] S. Komarneni, Hydrothermal preparation of the low expansion NZP family of crystals, Int. J. High Tech. Ceram. 4 (1988) 31–39.

[6] A.I. Kryukova, I.A. Korhunov, E.P. Moskvichev, V.A. Mitrofanova, A.I. Kryukova, I.A. Korhunov, E.P. Moskvichev, V.A. Mitrofanova, N.V. Vorobeva, G.N. Kazantsev, O.V. Skiba, Preparation and study of the crystal structure of the compounds of the $M_2{}^IM_2{}^{III}(PO_4)_3$ type, Russ. J. Inorg. Chem. 21 (9) (1976) 1408–1409.

[7] D.A. Rega, D.K. Agrawal, C.Y. Huang, H.A. McKinstry, Microstructure and microcracking behavior of barium zirconium phosphate ($BaZr_4P_6O_{24}$) ceramics, J. Mater. Sci. 27 (1992) 2406–2412.

[8] M. Varadaraju, U.V. Sugantha, G.V. Subba Rao, Synthesis and characterization of NZP phases, $AM'^{3+}M''^{4+}P_3O_{12}$, J. Solid State Chem. 111 (1994) 33–40.

[9] V.I. Petkov, A.I. Orlova, Crystal-chemical approach to predicting the thermal expansion of compounds in the NZP family, Inorg. Mater. 39 (10) (2003) 1013–1023.

[10] C.S. Yoon, J.H. Kim, C.K. Kim, K.S. Hong, Synthesis of low thermal expansion ceramics based on $CaZr_4(PO_4)_6$–Li_2O system, Mater. Sci. Eng. B79 (2001) 6–10.

[11] H.T. Hawkins, B.E. Scheezt, Monophonic sodium zirconium phosphate (NZP) as a host structure for the immobilization of reprocessed high-level commercial wastes, Environ. Issues Waste Manage. Technol. (1998) 709–715.

[12] Y. Seida, M. Yuki, K. Suzuki, T. Sawa, Sodium zirconium phosphate [NZP] as a host matrix for high level radioactive wastes, in: Mat. Res. Soc. Symp. Proc., vol. 757, Materials Research Society, II3.25, 2003, pp. 1–6.

[13] A.Y. Troole, S.V. Stefanovsky, L.D. Bogomolova, EPR of Fe^{3+} and Cr^{3+} ions in NZP ceramics, Mat. Res. Soc. Symp. Proc. 556 (1999) 99–106.

[14] F.J. Berry, N. Constantine, L.E. Smart, Synthesis and characterisation of Cr^{3+}-containing NASICON-related phases, Solid State Ionics 177 (2006) 2889–2896.

[15] V.I. Pet'kov, M.V. Sukhanov, Immobilisation of molybdenum from fuel reprocessing wastes into sodium zirconium phosphate ceramics, Czechoslovak J. Phys. 53 (Suppl.) (2003) A671–A676.

[16] V.I. Pet'kov, A.I. Orlova, I.G. Trubach, Y.A. Asabina, V.T. Demarin, V.S. Kurazhkovskaya, Immobilisation of nuclear waste materials containing different alkali elements into single-phase NZP-based ceramics, Czechoslovak J. Phys. 53 (Suppl.) (2003) A639–A648.

[17] A.I. Orlova, Isomorphism in d- and f-element phosphates having framework crystal structure and crystallochemical conception of NZP matrix for radionuclide immobilization, Czechoslovak J. Phys. 53 (Suppl.) (2003) A649–A655.

[18] E. Breval, H.A. McKinstry, D.K. Agrawal, New [NZP] materials for protection coatings. Tailoring of thermal expansion, J. Mater. Sci. 35 (2000) 3359–3364.

[19] M. Sugantha, N.R.S. Kumar, U.V. Varadaraju, Synthesis and leachability studies of NZP and eulytine phases, Waste Manage. 18 (1998) 275–279.

[20] G. Buvaneswari, U.V. Varadaraju, Low leachability phosphate lattices for fixation of select metal ions, Mater. Res. Bull. 35 (2000) 1313–1323.

[21] G. Buvaneswari, U.V. Varadaraju, Synthesis of new network phosphates with NZP structure, J. Solid State Chem. 145 (1999) 227–234.

[22] Y. Miyajima, T. Miyoshi, J. Tamaki, M. Matsuoka, Y. Yamamoto, C. Masquelier, M. Tabuchi, Y. Saito, H. Kageyama, Solubility range and ionic conductivity of large trivalent ion doped $Na_{1+x}M_xZr_{2-x}P_3O_{12}$ (M: In, Yb, Er, Y, Dy, Tb, Gd) solid electrolytes, Solid State Ionics 124 (1999) 201–211.

[23] O.P. Shrivastava, N. Kumar, R. Chourasia, Synthesis, crystallographic characterization and ionic conductivity of iron substituted sodium zirconium phosphate $Na_{1.2}Zr_{1.8}Fe_{0.2}(PO_4)_3$, J. Mater. Sci. 42 (2007) 2551–2556.

[24] H. Kageyama, N. Kamijo, T. Asai, Y. Saito, K. Ado, O. Nakamura, XAFS study of nasicon-related compounds, $Na_3Zr_{0.5}Co_{0.5}FeP_3O_{12}$ and $Na_3Zr_{0.5}Fe(II)_{0.5}Fe(III)P_3O_{12}$, Solid State Ionics 40–41 (1990) 350–356.

[25] Y. Saito, K. Ado, T. Asai, H. Kageyama, O. Nakamura, Ionic conductivity of NASICON-type conductors $Na_{1.5}M_{0.5}Zr_{1.5}(PO_4)_3$ (M: Al^{3+}, Ga^{3+}, Cr^{3+}, Sc^{3+}, Fe^{3+}, In^{3+}, Yb^{3+}, Y^{3+}), Solid State Ionics 58 (1992) 327–331.

[26] E. Breval, H.A. McKinstry, D.K. Agrawal, Synthesis and thermal expansion properties of the $Ca_{(1+x)/2}Sr_{(1+x)/2}Zr_4P_{6-2x}Si_{2x}O_{24}$ system, J. Am. Ceram. Soc. 81 (4) (1998) 962–1032.

[27] S. Tantri, S. Ushadevi, S.K. Ramasesha, High temperature X-ray studies on barium and strontium zirconium phosphate based low thermal expansion materials, Mater. Res. Bull. 37 (2002) 1141–1147.

[28] R. Roy, E.R. Vance, J. Alamo, [NZP] a new radiophase for ceramic nuclear waste forms, J. Mater. Res. Bull. 17 (5) (1982) 585.

[29] B.E. Scheed, D.K. Agrawal, E. Brewal, Sodium zirconium phosphate as a host structure for nuclear waste immobilization: a review, Waste Manage. 14 (6) (1994) 489.

[30] B.E. Scheed, R. Roy, in: W. Lutze, R.C. Ewing (Eds.), Radioactive Wastes Forms for the Future, 1988, p. 586.

[31] Y. Hirose, T. Fukasawa, D.K. Agrawal, B.E. Scheed, R. Nageswaran, J.A. Curtis, S.Y. Limaye, An alternative process to immobilize intermediate waste from LWR fuel reprocessing, in: WM 1999 Conference, 1999.

[32] V.I. Petkov, A.I. Orlova, G.N. Kazantsev, S.G. Samoilov, M.L. Spridonova, Thermal expansion in the Zr and 1-, 2-valent complex phosphates of $NaZr_2(PO_4)_3$ (NZP), J. Thermal Anal. Calorim. 66 (2001) 623–632.

[33] JCPDS Powder Diffraction Data File No. 71-0959, compiled by International Center for Diffraction Data, USA, 2000.

[34] A.C. Larson, R.B. Von Dreele, General Structure Analysis System Technical Manual LANSCE MS-H805, Los Almos National University LAUR, 2000, pp. 86–748.
[35] C. Verissimo, F.M.S. Garrido, O.L. Alves, P. Calle, A.M. Juarez, J.E. Iglesias, J.M. Rojo, Ionic conductivity and structural characterization of $Na_{1.5}Nb_{0.3}Zr_{1.5}(PO_4)_3$ with NASICON-type structure, Solid State Ionics 100 (1997) 127–134.
[36] K.V. Govindan Kutty, R. Asuvathraman, R. Sridhran, Thermal expansion studies on sodium zirconium phosphate family of compounds $A_{1/2}M_2(PO_4)_3$: effect of interstitial and framework cations, J. Mater. Sci. 33 (1998) 4007–4013.
[37] R.D. Shannon, C.D. Prewitt, Effective ionic radii in oxides and fluorides, Acta Crystallogr. Sect. B 25 (Pt. 5) (1969) 925–946.
[38] R. Brochu, M. Louer, M. Alami, M. Alqaraoui, D. Louer, Structure and thermal expansion of $KGe_2(PO_4)_3$, Mater. Res. Bull. 32 (1) (1997) 113–122.
[39] N. Bhatt, R. Vaidya, S.G. Patel, A.R. Jani, X-ray diffraction studies of 332 $NbTe_2$ single crystal, Bull. Mater. Sci. 27 (2004) 23–25.